Modular Battery-Integrated Power Electronics—Modelling, Advantages, and Challenges

Nima Tashakor[1], Jan Kacetl[1], Tomas Kacetl[1], Stefan Goetz
Technische Universität Kaiserslautern
Kaiserslautern, Germany
E-Mail: tashakor@eit.uni-kl.de, jan.kacetl@porsche-engineering.de, tomas.kacetl@porsche-engineering.de

Acknowledgements

The authors acknowledge the financial support by the Federal Ministry of Education and Research of Germany in the project “Open6GHub” (grant number: 16KISK004).

Keywords

«Batteries», «Estimation technique », «Modular Multilevel Converter», «Reconfigurable Batteries», «Fault Tolerance», «Average State-Space Model», «Parameter Estimation», «Charge Balancing», «Smart Batteries»

Abstract

Modular battery-integrated converters (dynamically reconfigurable modular batteries) are expanding into emerging applications. Although widely popular, we are yet to fully exploit their potential. This paper provides a critical discussion of the more neglected aspects with particular focus on electro mobility applications. It also provides insight on the challenges and/or concerns.

Introduction

Despite renewable energy generation expansion, growth of the electromobility sector, environmental incentives, and intensified research on the battery technology, many of the traditional challenges still persist. Today, an electric vehicle (EV) is powered by the series and parallel connection of literally hundreds of cells [1]. In addition to the increased capacity, a trend toward higher voltage levels is observed that results in increasing the share of series connections in batteries with the same energy capacity [2-4]. The advantages behind a higher voltage battery pack (i.e., 800 V) include lower weight, better efficiency, and faster charging [5]. However, higher pack voltages and more serial connections can also lead to stricter protection and safety requirements, more complex monitoring and balancing sub-systems, as well as lower efficiency of the inverters at partial load [6-8].
Recent developments in power electronics have enhanced the performance of the low-voltage transistors while continuously reducing their prices, paving the way for emergence of new concepts such as battery-integrated modular multilevel converters, also known as dynamically reconfigurable batteries [9-13]. These systems break the conventionally hard-wired battery pack into multiple modules and integrate them with power electronics to achieve dynamic reconfiguration. There are quite well-known advantages to a modular battery system, such as better balancing, fault tolerance, and controllability as well as faster output regulation [14-16]. Furthermore, it is proven that the overall efficiency can be improved [17, 18]. However, considering the available degree of freedom in such systems, they have yet to fully achieve their potential. Additionally, as popular as these systems are, there are still many aspects that are not fully investigated such as their effect on battery aging, the current profiles and its effect, other topologies, and optimal module sizing.

[1] The first three authors have contributed equally to the paper.

Discussion of Possible Macro and Micro Topologies

Reconfigurable batteries and battery-integrated cascaded converters are not a new concept and there are many different macro and micro topologies available in the literature [19]. Different string connections can provide DC, single-phase, and multi-phase structures with specific features [10]. It is possible to place only one connection between every two adjacent modules (e.g., in case of half-bridge or bi-directional full-bridge) allowing for merely bypass and series connection in the string or there can be more than one point of connection (e.g., diode-clamped [20, 21], FET-clamped [22], or topologies with higher number of switches [23]). Since a review of different topologies is not the purpose of this work, we only discuss the critical points of the more feasible approaches to battery-integrated systems with particular focus on electromobility, but more detailed reviews of different topologies can be found in the literature [24-26].

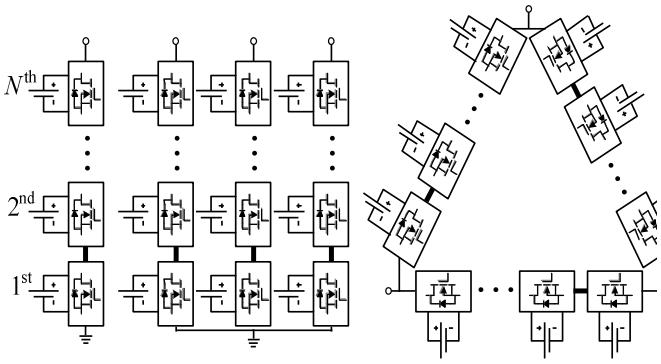

(a) (b) (c)

Fig. 1. (a) Single-phase single-arm structure, (b) three-phase single-arm structure with star connection, (c) three-phase single-arm structure with delta connection

AC Structures

In general, all the available AC topologies for the modular multilevel converters are also usable with reconfigurable AC batteries, and indeed a large body of research focusses on developing or modifying available control and algorithms for battery-integrated inverters [9, 27, 28]. However, while the double-arm MMC topology is very useful in capacitor-based modules to create a buffer between the main source of energy (the DC links), it offers almost no practical advantage in case of battery-integrated modules, needs higher numbers of battery modules, and increases the isolation voltage requirement as well as cost of the monitoring/balancing/protection subsystems.

The main idea behind the dual-arm topology is to provide a floating AC output, while the voltage sum of both strings remains constant, and minimize the size of the module capacitances as the intermediary energy storage. However, with batteries inside the modules, the main sources of energy are the batteries, and there is no need for a double-arm structure. Comparingly, the cascaded full-bridge topology in a single-arm structure can achieve the same output voltage levels, with the same number of semiconductors, while reducing the isolation voltage, the number of battery modules, and monitoring as well as protection requirements to half. A duality of this condition also holds true for the dual-arm cascaded full-bridge topologies with parallel function [29] and the single-arm double full-bridge structure [12]. It is possible to connect multiple strings in different structures, e.g., star and delta structures as Fig. 1 illustrates. Furthermore, Fig. 2 depicts the two interesting module topologies for AC application. The double-full-bridge topology can offer parallel connectivity, whereas the single-full-bridge can only provide bypass and series connections [30].

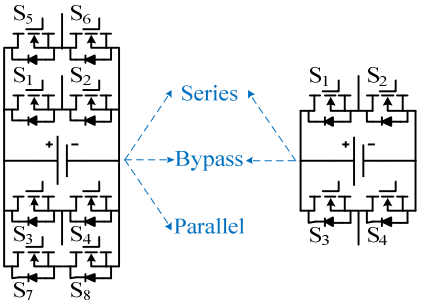

Fig. 2. Recommended module topologies for single-arm structures

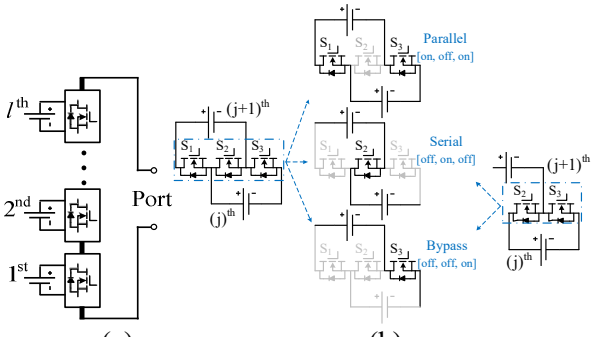

(a) (b)

Fig. 3. (a) Generic structure of a string; (b) simplest module topologies with possible operation modes

DC Structures

Many applications, also in electromobility, do not aim for a reconfigurable AC battery as the overall architecture, including one or more separate DC outputs for auxiliaries, poses different constraints. A more cost-effective approach can be a reconfigurable DC battery modulating the DC-link voltage, while a conventional inverter generates necessary AC voltage [31]. For a DC structure with integrated batteries, normally only a single string suffices, but there are still many debates about the sizing (which will be discussed in Section III) as well as the module topology.

For DC structures, the minimum available connection modes are bypass and series, which can be achieved with the minimum of two switches per module in half-bridge topology. However, parallel connectivity in addition to the previous connection modes is preferred in many applications, since it can offer better efficiency, reduce ripple issues, increase the rated power, average the load better across modules, and contribute to balancing of the modules. Although it is possible to achieve parallel function in some cases with an additional diode in diode-clamped topologies, the resulting efficiency is not ideal. For more efficiency, parallel connection as well as previous bypass and series modes and thus at least three switches are necessary. Fig. 3(a) illustrates a generic form of a DC string, and Fig. 3(b) depicts the two simplest module topologies [32]. More complex circuits can offer additional capabilities, e.g., fault protection [33, 34].

Average State-Space Model of a String

Modelling each battery with a series resistance as well as multiple RC networks, the string voltage at each instance can be calculated per

$$V_{\text{string}}(t) = \boldsymbol{S}^T(t) \times \left(\boldsymbol{V_{oc}}(t) - \boldsymbol{R_0}(t) i_{\text{string}} - \boldsymbol{V_{RC,1}} - \boldsymbol{V_{RC,2}} - \cdots\right), \tag{1}$$

where S^T is the modules state vector and can be $+1$ for positive series, -1 for negative series, and 0 for bypass/parallel [35]. Additionally, $\boldsymbol{V_{oc}^T} = [V_{oc,1}, \ldots, V_{oc,N}]$ and $\boldsymbol{R_0^T} = [R_{0,1}, \ldots, R_{0,N}]$ are respectively the vectors of open-circuit voltage as well as the internal resistance, and $\boldsymbol{V_{RC,i}}$ is the vector of voltages across the i^{th} RC network. Lastly, $\times$ denotes the cross product. The derivation of $\boldsymbol{V_{RC,i}}$ is

$$\frac{\mathrm{d}\boldsymbol{V_{RC,i}}}{\mathrm{d}t} = \boldsymbol{S}.\frac{\boldsymbol{1}}{\boldsymbol{C_i}}.i_{\text{string}} - \frac{\boldsymbol{V_{RC,i}}}{\boldsymbol{R_i C_i}}, \tag{2}$$

where $\boldsymbol{R_i^T} = [R_{i,1}, \ldots, R_{i,N}]$, and $\boldsymbol{C_i^T} = [C_{i,1}, \ldots, C_{i,N}]$ are respectively the vector of the RC network resistances and capacitances. Additional RC networks can similarly be included into the model for better accuracy.

As (1) and (2) suggest, the equations have a discrete form depending on the state vector $\boldsymbol{S}$. However, a continuous derivation is possible through averaging the states as

$$V_{\text{string}}(t) = \boldsymbol{M}^T(t) \times \left(\overbrace{\boldsymbol{V_{oc}}(t) - \boldsymbol{R_0}(t).i_{\text{string}} - \boldsymbol{V_{RC,1}} - \boldsymbol{V_{RC,2}} - \cdots}^{\boldsymbol{V_t}}\right), \tag{4}$$

$$\frac{\mathrm{d}\boldsymbol{V_{RC,i}}}{\mathrm{d}t} = \boldsymbol{M}.\frac{\boldsymbol{1}}{\boldsymbol{C_i}}.i_{\text{string}} - \frac{\boldsymbol{V_{RC,i}}}{\boldsymbol{R_i C_i}}, \tag{5}$$

where $\boldsymbol{M^T} = [m_1, m_2, \ldots, m_N]$ is the vector of the modulation indices of the modules, $\left(\boldsymbol{M}.\frac{\boldsymbol{1}}{\boldsymbol{C_i}}\right)^{\boldsymbol{T}} = \left[\frac{m_1}{C_{1,1}}, \frac{m_2}{C_{1,2}}, \ldots, \frac{m_N}{C_{1,N}}\right]$ represents the dot product of the vectors $\boldsymbol{M}$ and $\frac{\boldsymbol{1}}{\boldsymbol{C_i}}$, and $\boldsymbol{V_t^T} = [V_{t,1}, \ldots, V_{t,N}]$ is the vector of the terminal voltage of the battery modules .

With a LC low-pass filter (L_{LPF} and C_{LPF}) across the string as Fig. 4 illustrates, it is possible to write the average state space equations per

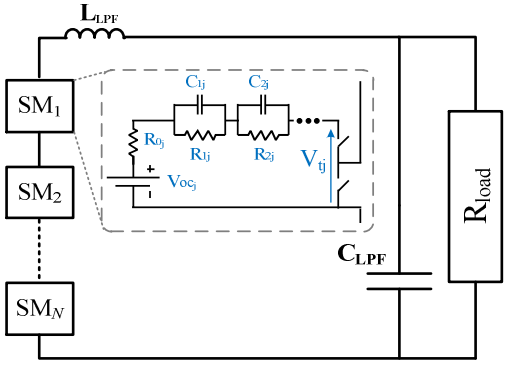

Fig. 4. Circuit of the modeled string

$$\dot{X} = \boldsymbol{A} \times \boldsymbol{X} + \boldsymbol{B} \times \boldsymbol{V_t}, \quad (6)$$

where $\boldsymbol{X^T} = [i_{\text{string}}, V_o\,]$ is the vector of the state variables, and $\boldsymbol{A}$ and $\boldsymbol{B}$ are defined per

$$\boldsymbol{A} = \begin{bmatrix} \left(-\frac{1}{L_{dc}}\right)(Nr_{\text{sw}} + R_{\text{LPF}}) & \frac{-1}{L_{\text{LPF}}} \\ \frac{1}{C_{\text{LPF}}} & -\frac{1}{(R_{\text{Load}} C_{\text{LPF}})} \end{bmatrix}, \quad (7)$$

$$\boldsymbol{B} = \begin{bmatrix} \boldsymbol{M^T} \frac{1}{L_{LPF}} \\ 0 \ldots 0 \end{bmatrix}. \quad (8)$$

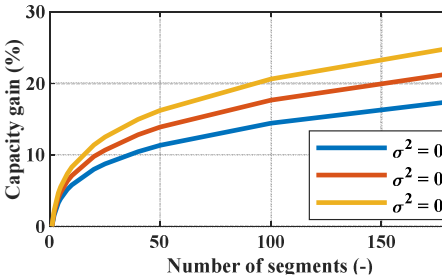

Fig. 5. Average capacity gain of cell string segmenting (μ = 4 Ah, σ^2 = 0.05, σ^2 = 0.07, σ^2 = 0.09)

Therefore, at each instance, first the $\boldsymbol{V_{RC,i}}$ values are updated using (5), then the new terminal voltages of each module are calculated using (4), and lastly, the new operating point of the string is calculated per (6).

Unknown Caveats, Challenges, Trade-Offs, and Potentials

Sizing Statistics and Necessary Trade-offs

The capacity of hard-wired battery packs is limited by the weakest cell in the string. Thus, the capacity follows the law of minimum [36, 37]. This limitation to the weakest element leads to a large loss of capacity in large batteries with many cells in series. It grows with the number of cells and therefore aggravates for high-voltage packs such as in grid storage and electric vehicles. The battery pack mean usable capacity is calculated per

$$E(Q_n) = \int_{-\infty}^{\infty} Q \cdot f(Q, \mu, \sigma) \cdot \left(1 - F(Q, \mu, \sigma)\right)^{n-1} dQ, \quad (9)$$

where Q is the ampere-hour capacity, f is the cell capacity distribution function with Gaussian distribution, F is the cell capacity cumulated distribution function, μ is the mean value, σ is the standard deviation, and n is the number of cells in series. To minimize the effect, long strings require high-quality cells with minimal parameter variation. However, low manufacturing tolerances and cell pre-selection increases the overall cost. Still, even initially perfectly matching cells age differently, leading to even further increase of the tolerances in a battery pack [38].

Although multiple active balancing techniques focused on increasing the usable battery pack capacity exist, they can only balance charge but not power, heating, or ageing. Furthermore, simple passive balancing still dominates in the industry. Reconfigurable battery packs can fully control the current flow in the battery, thus actively balance the pack on the module level. Such a battery pack splits the long hard-wired cell string into shorter segments which leads to gain in the usable capacity, as Fig. 5 depicts. With additional balancing capability, the usable life of the overall battery pack can be increased, as further extreme tolerances between the modules' capacities can be neutralized.

Active regulation of each module can provide the opportunity to integrate the battery management functions into the control loops of each module and offset the cost of additional power electronics circuitry. However, increasing the segments can also increase complexity along with cost, and the additional electronics can reduce the efficiency of the energy storage system. Therefore, there is still a trade-off between the number of segments and the gain in usable capacity.

Parallel Connection, Better Load share

In contrast to traditional module topologies with series and bypass connectivity, topologies with parallel connectivity offer substitution of bypassing by clustering in parallel groups [39]. Elimination of inactive states and distribution of load by paralleling effectively reduces root-mean square (RMS) value of the module load, which consequently decreases string impedance and increases efficiency [40]. Furthermore, parallel distribution prevents temporal overloading of the battery at phase currents exceeding their maximum discharge rates [41].

With simplification, the average equivalent resistance of the reconfigurable battery, respectively, with and without parallel mode can be approximated per

$$R_{\text{eq,without}} \approx \boldsymbol{M^T} \times \boldsymbol{R_{bt}} + N_1 r_{\text{sw}}, \quad (10)$$

$$R_{\text{eq,with}} \approx \frac{\boldsymbol{M^T}}{(1-\boldsymbol{M^T}).N} \times \boldsymbol{R_{bt}} + N_2 r_{\text{sw}}, \tag{11}$$

which confirm that with comparable die area for the transistors, the parallel mode can help reducing the conduction loss. In (10) and (11), $\boldsymbol{R_{bt}} = \boldsymbol{R_0} + \boldsymbol{R_1} + \cdots$ is the vector of equivalent resistance of the battery model shown in Fig. 4. Additionally, N_1 and N_2 are the number of semi-conductors derated by their current at each moment and can depend on the topology as well as the modulation. However, in many cases assuming $N_1 \approx N_2$ and equal to total number of modules (N) is a reasonable assumption [29].

The distribution of the load among paralleled modules is governed by voltage differences between modules, which are typically kept minimal through controller's effort, and proportions between battery impedance and their interconnection paths, typically low enough for sufficiently low differences [42]. Dependent on the resistance ratio of interconnection and batteries in the modules paralleling a high number of modules pushes the majority of the load towards outer modules of the parallel group, whereas the inner modules close to middle of the group remain lightly loaded [43].

Fig. 6 displays distribution of the load share in a reconfigurable battery with ten modules, where the outer modules (Modules 1, 2, 9, and 10) can take significantly more load than modules in the center of the parallel cluster (Modules 5 and 6). The parabolic character of the current distribution is discussed in greater detail in [43]. Higher load share will discharge the outer modules faster, which consequently increase the balancing current (i.e., a circulating current between two adjacent modules), until an equilibrium is achieved.

Higher Output Quality/Better Output Discretization/Lower Filter

Unlike conventional two-level converters, modular reconfigurable systems provide the output voltage in discrete steps. The voltage discretization itself brings about lower voltage derivations resulting in output filter reduction. In addition, modularization allows the implementation of low-voltage semiconductor switches with high switching dynamics to increase the module switching rate. Furthermore, proper modulation techniques, such as phase-shifted carrier (PSC) modulation further increase the effective output frequency N times [30, 44]. The lower voltage deviation, high module switching dynamic, and PSC modulation can reduce the requirement on the output filter, as described by

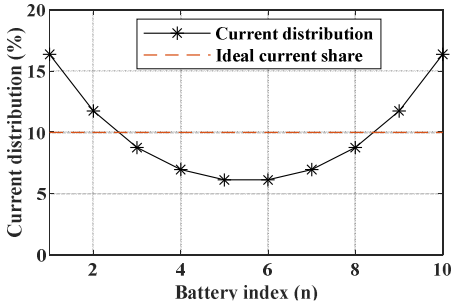

Fig. 6. Distribution of load in parallel group

$$\boldsymbol{L} \approx \frac{\boldsymbol{V_{BP}}}{\boldsymbol{N^2 . f_{sw}}}, \tag{12}$$

where V_{BP} is the battery pack maximal voltage and f_{sw} is the module switching rate.

Such a feature is easily evaluated by comparing the reconfigurable system (as shown in Fig. 4) to a conventional buck converter. Typically, the filtering inductor is designed with respect to the switching rate, the duty cycle (D), input (V_{in}) and output (V_{out}) voltages to restrict the certain current ripple (ΔI_L) below a certain threshold per

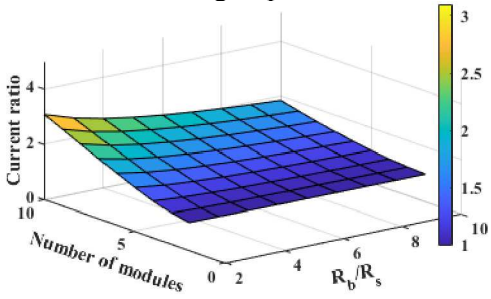

Fig. 7. Influence of impedances and number of moduels

$$\Delta \boldsymbol{I_L} \leq \frac{\boldsymbol{D(V_{in}-V_{out})}}{\boldsymbol{f_{sw}L}}. \tag{13}$$

The highest current ripple in a conventional buck converter supplied from a battery pack ($V_{\text{in}} = V_{\text{BP}}$) occurs when $D = 0.5$ at $V_{\text{out}} = V_{\text{in}}/2$. In a reconfigurable battery, the highest ripple occurs when the difference between the input and the output voltage is equal to the half of the module voltage, e.g., $V_{\text{out}} - V_{\text{in}} = V_m/2 = V_{BP}/2N$. At such an operating point, the reconfigurable

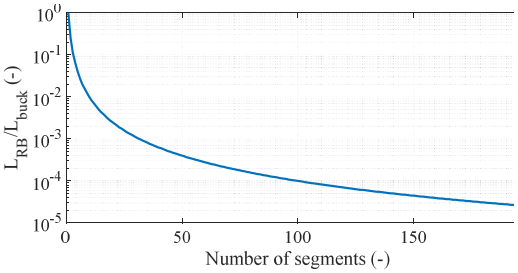

Fig. 8. Output filter reduction with battery pack segmenting

system switches between two voltage levels nearest to the output voltage with equal conduction times t_{on} and t_{off}, thus exhibits an equivalent duty cycle of 50% ($D = 0.5$). Comparing the current ripples for both topologies, and considering the same maximum threshold and the switching rate, we obtain

$$\frac{0.5\left(V_{\mathrm{BP}}-\frac{V_{\mathrm{BP}}}{2}\right)}{f_{\mathrm{sw}}L_{\mathrm{buck}}} = \frac{0.5\frac{V_{\mathrm{BP}}}{2N}}{Nf_{sw}L_{\mathrm{RB}}}, \tag{14}$$

which can be simplified to

$$\frac{L_{\mathrm{RB}}}{L_{\mathrm{buck}}} = \frac{1}{N^2}. \tag{15}$$

Equation (15) confirms that the size of the filtering inductor has an inversed squared relation with the number of modules. Consequent to the improved quality and increased effective switching frequency at the output, the size of the output filter is reduced. Fig. 8 illustrates the ratio of such a reduction compared to a normal hard-wired battery pack supplying a buck converter.

Estimation Techniques to Simplify Monitoring

Reconfigurable batteries offer many advantages over conventional battery packs. However, some functions such as the protection and monitoring are still necessary, which added to the more complex circuitry necessitate more sensors as well as higher-bandwidth communication channels [30, 41]. On the other hand, similar to MMCs with capacitors, knowing the exact state of each module in addition to the output voltage and current can provide sufficient information to estimate the state of each module without any direct measurement at the module level. However, on the contrary to modules with capacitors, with batteries the terminal voltage is not the only necessary parameter that needs monitoring [45]. Two important parameters that deserve monitoring are the equivalent resistance for age and under-load state-of-charge (SOC) estimation as well as the open-circuit voltage, which is a direct indicator of SOC [46].
Theoretically, it is possible to use the available methods for MMCs with capacitors to estimate the terminal voltage of the batteries and then use the terminal voltage, the module state, and the arm current to estimate other parameters of the battery such as open-circuit voltage as well as its electrical equivalent

Table I: Generic algorithms for parameter estimation of reconfigurable batteries

Case	Updatable parameters	Process / Comment
Battery has been idle for a long time (few hours)	V_{oc}	- After a long period of time V_{oc} can be measured through terminal voltage $V_{oc} = V_t$
Fast current variations (few milliseconds)	R_0, τ_1, R_1	- There is an immediate jump due to R_0: $R_0 = \frac{\Delta v_1}{\Delta i}$ - The time-constant τ_1 can be calculated from V_t shape - After few ms, the RC network reaches steady state, and R_1 can be calculated per $R_1 = \frac{\Delta v_2}{\Delta i} - R_0$
Slow current variations (few seconds)	R_2, τ_2	- With slow variations of current, the first RC network response is negligible, and τ_2 can be approximated from V_t - Neglecting SOC variations, the resistance can be calculated per $R_2 = \frac{\Delta v_3}{\Delta i_3} - R_0 - R_1$
⋮		
Constant current, in steady-state condition	V_{oc}	- The only variation is due to the SOC changes, and open-circuit voltage is $V_{oc} = V_t - iR_0 - iR_1 - \cdots$

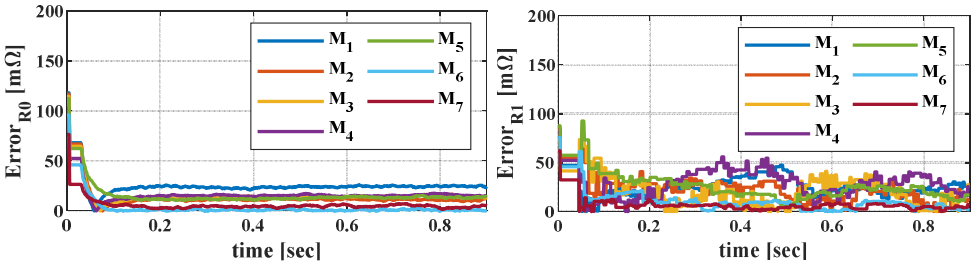

Fig. 9. Example of estimation of the resistances using sequential estimation

circuit [47]. As long as the switching frequency of the modules is considerably higher than the battery time constants, it is possible to decouple the terminal voltage of each module by just measuring the output voltage. However, the effect of the voltage sensor must be compensated [48] per

$$v_{\text{comp}} = v_{\text{meas}} + \frac{\Delta v_{\text{meas}}}{1-\exp\left(-\frac{\Delta t}{\tau}\right)}. \quad (16)$$

Table I presents a generic algorithm for a sequential parameter estimation approach, while Fig. 9 offers an example result of applying the provided procedure in an experimental data to estimate $\boldsymbol{R_0}$ vector depicted in Fig. 4.

Current Ripple Profile and Its Effect on Aging

The spectrum of the module load is strongly affected by the character of the terminal load. Batteries with AC output feature dominant components of the fundamental phase frequency, especially the second harmonic, which is further accompanied by an increased spectrum around the switching rate. The current ripple is typically subject to filtering in supplemented DC link capacitors on each module [49]. Alternatively, the current ripple suppression might be incorporated in the control objectives of the reconfigurable battery [40].

Highly rippled load of the module, as shown in Fig. 10, eventually increases losses in the battery cells and accelerates their ageing [50]. Recent studies show, however, that high-frequency ripple can mostly flow through the electrode capacitance without extensive activation of faradaic processes on the electrode-electrolyte interface, which reduces cycling of the battery and consequently ageing [51]. The behavior of the electrode capacitance is described in Randles' model in Fig. 11, where faradaic processes are modeled as a constant-phase element (Warburg impedance Z_{W}) and a charge transfer resistance R_{ct}. The faradaic path is bypassed by the electrode double layer capacitance C_{dl}, which forms the high pass characteristic of the cell impedance. For higher frequencies, the charge cumulated in the capacity C_{dl} is sufficient to feed the load ripple without extensive fluctuation of the voltage across the charge transfer resistance R_{ct} (electrode-electrolyte interface respectively). Voltage across the interface drives kinetics of the primary electrochemical reaction, but also increases kinetics of side reactions. Therefore, reduced fluctuation of the interface potential, decreases the additional ageing of the battery call connected to the rippled load [52]. In summary, shifting the ripple profile of the load current to higher frequencies can lead to a reduction in aging.

Conclusion

This paper investigates key aspects of the reconfigurable batteries through statistical analysis, discussion, simulations, and experiments. The paper investigates the trade-offs between module size as well as the number of serial cells and analyzes the output voltage quality as well as filter size of reconfigurable batteries. Furthermore, it discusses the effect of parallel connection in reducing the effective impedance of the system, and the uneven distribution of the load current among paralleled modules. The possibility of state estimation to reduce the cost of monitoring system is proposed, with an example case of the experimental results. Lastly, we debate the concept of exploiting the double-layer capacitance of the battery to reduce the aging.

References

[1] A. N. Link, O'Connor, A. C., Scott, T. J., "Battery Technology for Electric Vehicles.," *London:*

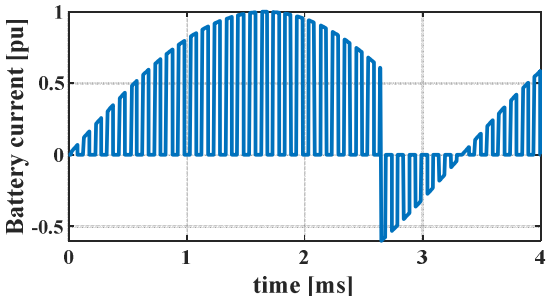

Fig. 10. Current waveform of a battery cell in a cascaded full-bridge topology

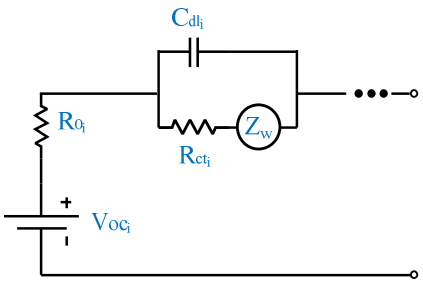

Fig. 11. Randles' equivalent circuit of the battery model

Routledge, , 2015, doi: https://doi.org/10.4324/9781315749303.

[2] S. Absar, W. Taha, and A. Emadi, "Efficiency Evaluation of Six-Phase VSI and NSI for 400V and 800V Electric Vehicle Powertrains," presented at the IECON 2021 – 47th Annual Conference of the IEEE Industrial Electronics Society, 13-16 Oct. 2021, 2021.

[3] I. Aghabali, J. Bauman, P. J. Kollmeyer, Y. Wang, B. Bilgin, and A. Emadi, "800-V Electric Vehicle Powertrains: Review and Analysis of Benefits, Challenges, and Future Trends," *IEEE Transactions on Transportation Electrification,* vol. 7, no. 3, pp. 927-948, 2021, doi: 10.1109/TTE.2020.3044938.

[4] A. Allca-Pekarovic, P. J. Kollmeyer, P. Mahvelatishamsabadi, T. Mirfakhrai, P. Naghshtabrizi, and A. Emadi, "Comparison of IGBT and SiC Inverter Loss for 400V and 800V DC Bus Electric Vehicle Drivetrains," in *2020 IEEE Energy Conversion Congress and Exposition (ECCE)*, 11-15 Oct. 2020 2020, pp. 6338-6344, doi: 10.1109/ECCE44975.2020.9236202.

[5] C. Jung, "Power Up with 800-V Systems: The benefits of upgrading voltage power for battery-electric passenger vehicles," *IEEE Electrification Magazine,* vol. 5, no. 1, pp. 53-58, 2017, doi: 10.1109/MELE.2016.2644560.

[6] J. Zhang, Z. Wang, P. Liu, and Z. Zhang, "Energy consumption analysis and prediction of electric vehicles based on real-world driving data," *Applied Energy,* vol. 275, p. 115408, 2020.

[7] M. Jaensch, J. Kacetl, T. Kacetl, and S. Götz, "Modulation index improvement by intelligent battery," Patent US10784698B2, 2020.

[8] Y. Yang, Q. Ye, L. J. Tung, M. Greenleaf, and H. Li, "Integrated Size and Energy Management Design of Battery Storage to Enhance Grid Integration of Large-Scale PV Power Plants," *IEEE Transactions on Industrial Electronics,* vol. 65, no. 1, pp. 394-402, 2018.

[9] C. Gan, Q. Sun, J. Wu, W. Kong, C. Shi, and Y. Hu, "MMC-Based SRM Drives With Decentralized Battery Energy Storage System for Hybrid Electric Vehicles," *IEEE Transactions on Power Electronics,* vol. 34, no. 3, pp. 2608-2621, 2019, doi: 10.1109/TPEL.2018.2846622.

[10] N. Tashakor, E. Farjah, and T. Ghanbari, "A Bidirectional Battery Charger With Modular Integrated Charge Equalization Circuit," *IEEE Transactions on Power Electronics,* vol. 32, no. 3, pp. 2133-2145, 2017, doi: 10.1109/TPEL.2016.2569541.

[11] Y. Li and Y. Han, "A Module-Integrated Distributed Battery Energy Storage and Management System," *IEEE Transactions on Power Electronics,* vol. 31, no. 12, pp. 8260-8270, 2016, doi: 10.1109/TPEL.2016.2517150.

[12] S. M. Goetz, Z. Li, X. Liang, C. Zhang, S. M. Lukic, and A. V. Peterchev, "Control of modular multilevel converter with parallel connectivity—Application to battery systems," *IEEE Transactions on Power Electronics,* vol. 32, no. 11, pp. 8381-8392, 2016.

[13] Z. Zedong, W. Kui, X. Lie, and L. Yongdong, "A Hybrid Cascaded Multilevel Converter for Battery Energy Management Applied in Electric Vehicles," *Power Electronics, IEEE Transactions on,* vol. 29, no. 7, pp. 3537-3546, 2014, doi: 10.1109/TPEL.2013.2279185.

[14] S. Ali, Z. Ling, K. Tian, and Z. Huang, "Recent Advancements in Submodule Topologies and Applications of MMC," *IEEE Journal of Emerging and Selected Topics in Power Electronics,* pp. 1-1, 2020, doi: 10.1109/JESTPE.2020.2990689.

[15] T. Zheng *et al.*, "A Novel Z-Type Modular Multilevel Converter with Capacitor Voltage Self-Balancing for Grid-Tied Applications," *IEEE Transactions on Power Electronics,* pp. 1-1, 2020, doi: 10.1109/TPEL.2020.2997991.

[16] S. Xu, "A New Multilevel AC/DC Topology Based H-Bridge Alternate Arm Converter," *IEEE Access,* vol. 8, pp. 57997-58005, 2020, doi: 10.1109/ACCESS.2020.2982202.

[17] M. Quraan, P. Tricoli, S. D'Arco, and L. Piegari, "Efficiency assessment of modular multilevel converters for battery electric vehicles," *IEEE Transactions on Power Electronics,* vol. 32, no. 3, pp. 2041-2051, 2016.

[18] N. Tashakor, B. Arabsalmanabadi, L. O. Cervera, E. Hosseini, K. Al-Haddad, and S. Goetz, "A Simplified Analysis of Equivalent Resistance in Modular Multilevel Converters with Parallel Functionality," presented at the IECON 2020 The 46th Annual Conference of the IEEE Industrial Electronics Society, 18-21 Oct. 2020, 2020.

[19] M. Quraan, T. Yeo, and P. Tricoli, "Design and Control of Modular Multilevel Converters for Battery Electric Vehicles," *IEEE Transactions on Power Electronics,* vol. 31, no. 1, pp. 507-517, 2016, doi: 10.1109/TPEL.2015.2408435.

[20] T. Zheng *et al.*, "A Novel High-Voltage DC Transformer Based on Diode-Clamped Modular Multilevel Converters With Voltage Self-Balancing Capability," *IEEE Transactions on Industrial Electronics,* vol. 67, no. 12, pp. 10304-10314, 2020, doi: 10.1109/TIE.2019.2962486.

[21] N. Tashakor, M. Kilictas, E. Bagheri, and S. Goetz, "Modular Multilevel Converter with Sensorless Diode-Clamped Balancing through Level-Adjusted Phase-Shifted Modulation," *IEEE Transactions on Power Electronics,* pp. 1-1, 2020, doi: 10.1109/TPEL.2020.3041599.

[22] Y. Jin *et al.*, "A Novel Submodule Voltage Balancing Scheme for Modular Multilevel Cascade Converter—Double-Star Chopper-Cells (MMCC-DSCC) based STATCOM," *IEEE Access,* 2019.
[23] J. Xu, J. Li, J. Zhang, L. Shi, X. Jia, and C. Zhao, "Open-loop voltage balancing algorithm for two-port full-bridge MMC-HVDC system," *International Journal of Electrical Power & Energy Systems,* vol. 109, pp. 259-268, 2019/07/01/ 2019, doi: https://doi.org/10.1016/j.ijepes.2019.01.032.
[24] J. Fang, F. Blaabjerg, S. Liu, and S. M. Goetz, "A Review of Multilevel Converters With Parallel Connectivity," *IEEE Transactions on Power Electronics,* vol. 36, no. 11, pp. 12468-12489, 2021, doi: 10.1109/TPEL.2021.3075211.
[25] A. K. Bhattacharjee, N. Kutkut, and I. Batarseh, "Review of Multiport Converters for Solar and Energy Storage Integration," *IEEE Transactions on Power Electronics,* vol. 34, no. 2, pp. 1431-1445, 2019, doi: 10.1109/TPEL.2018.2830788.
[26] S. Debnath, J. Qin, B. Bahrani, M. Saeedifard, and P. Barbosa, "Operation control and applications of the modular multilevel converter: A review," *IEEE Trans. Power Electron,* vol. 30, no. 1, pp. 37-53, 2015.
[27] N. Li, F. Gao, T. Hao, Z. Ma, and C. Zhang, "SOH Balancing Control Method for the MMC Battery Energy Storage System," *IEEE Transactions on Industrial Electronics,* vol. 65, no. 8, pp. 6581-6591, 2018, doi: 10.1109/TIE.2017.2733462.
[28] L. Baruschka and A. Mertens, "Comparison of Cascaded H-Bridge and Modular Multilevel Converters for BESS application," presented at the 2011 IEEE Energy Conversion Congress and Exposition, 17-22 Sept. 2011, 2011.
[29] N. Tashakor, F. Iraji, and S. G. Goetz, "Low-Frequency Scheduler for Optimal Conduction Loss in Series/Parallel Modular Multilevel Converters," *IEEE Transactions on Power Electronics,* pp. 1-1, 2021, doi: 10.1109/TPEL.2021.3110213.
[30] N. Tashakor, Z. Li, and S. M. Goetz, "A Generic Scheduling Algorithm for Low-Frequency Switching in Modular Multilevel Converters With Parallel Functionality," *IEEE Transactions on Power Electronics,* vol. 36, no. 3, pp. 2852-2863, 2021, doi: 10.1109/TPEL.2020.3018168.
[31] J. Kacetl, J. Fang, T. Kacetl, N. Tashakor, and S. Goetz, "Design and Analysis of Modular Multilevel Reconfigurable Battery Converters for Variable Bus Voltage Powertrains," *IEEE Transactions on Power Electronics,* pp. 1-1, 2022, doi: 10.1109/TPEL.2022.3179285.
[32] N. Tashakor, Z. Li, and S. M. Goetz, "A Generic Scheduling Algorithm for Low-Frequency Switching in Modular Multilevel Converters with Parallel Functionality," *IEEE Transactions on Power Electronics,* pp. 1-1, 2020, doi: 10.1109/TPEL.2020.3018168.
[33] D. Ronanki and S. S. Williamson, "Modular multilevel converters for transportation electrification: Challenges and opportunities," *IEEE Transactions on Transportation Electrification,* vol. 4, no. 2, pp. 399-407, 2018.
[34] Z. Li, R. Lizana, S. Sha, Z. Yu, A. V. Peterchev, and S. Goetz, "Module Implementation and Modulation Strategy for Sensorless Balancing in Modular Multilevel Converters," *IEEE Transactions on Power Electronics,* 2018.
[35] S. M. Goetz, Z. Li, A. V. Peterchev, X. Liang, C. Zhang, and S. M. Lukic, "Sensorless scheduling of the modular multilevel series-parallel converter: enabling a flexible, efficient, modular battery," presented at the 2016 IEEE Applied Power Electronics Conference and Exposition (APEC), 2016.
[36] M. A. Hannan, M. M. Hoque, A. Hussain, Y. Yusof, and P. J. Ker, "State-of-the-Art and Energy Management System of Lithium-Ion Batteries in Electric Vehicle Applications: Issues and Recommendations," *IEEE Access,* vol. 6, pp. 19362-19378, 2018, doi: 10.1109/ACCESS.2018.2817655.
[37] W. Waag, C. Fleischer, and D. U. Sauer, "Critical review of the methods for monitoring of lithium-ion batteries in electric and hybrid vehicles," *Journal of Power Sources,* vol. 258, pp. 321-339, 2014/07/15/ 2014, doi: https://doi.org/10.1016/j.jpowsour.2014.02.064.
[38] M. Baumann, L. Wildfeuer, S. Rohr, and M. Lienkamp, "Parameter variations within Li-Ion battery packs – Theoretical investigations and experimental quantification," *Journal of Energy Storage,* vol. 18, pp. 295-307, 2018/08/01/ 2018, doi: https://doi.org/10.1016/j.est.2018.04.031.
[39] S. M. Goetz, A. V. Peterchev, and T. Weyh, "Modular Multilevel Converter With Series and Parallel Module Connectivity: Topology and Control," *IEEE Transactions on Power Electronics,* vol. 30, no. 1, pp. 203-215, 2015, doi: 10.1109/TPEL.2014.2310225.
[40] Z. Li, R. Lizana, S. M. Lukic, A. V. Peterchev, and S. M. Goetz, "Current Injection Methods for Ripple-Current Suppression in Delta-Configured Split-Battery Energy Storage," *IEEE Transactions on Power Electronics,* vol. 34, no. 8, pp. 7411-7421, 2019, doi: 10.1109/TPEL.2018.2879613.
[41] B. Arabsalmanabadi, N. Tashakor, Y. Zhang, K. Al-Haddad, and S. Goetz, "Parameter Estimation of Batteries in MMCs with Parallel Connectivity using PSO," presented at the IECON 2021 – 47th Annual Conference of the IEEE Industrial Electronics Society, 13-16 Oct. 2021, 2021.

[42] G. Gunlu, "Dynamically Reconfigurable Independent Cellular Switching Circuits for Managing Battery Modules," *IEEE Transactions on Energy Conversion,* vol. 32, no. 1, pp. 194-201, 2017, doi: 10.1109/TEC.2016.2616190.

[43] Y. Zhu, W. Zhang, J. Cheng, and Y. Li, "A novel design of reconfigurable multicell for large-scale battery packs," presented at the 2018 International Conference on Power System Technology (POWERCON), 6-8 Nov. 2018, 2018.

[44] N. Tashakor and M. Khooban, "An Interleaved Bi-Directional AC–DC Converter With Reduced Switches and Reactive Power Control," *IEEE Transactions on Circuits and Systems II: Express Briefs,* vol. 67, no. 1, pp. 132-136, 2020, doi: 10.1109/TCSII.2019.2903389.

[45] D. N. T. How, M. A. Hannan, M. S. H. Lipu, K. S. M. Sahari, P. J. Ker, and K. M. Muttaqi, "State-of-Charge Estimation of Li-Ion Battery in Electric Vehicles: A Deep Neural Network Approach," *IEEE Transactions on Industry Applications,* vol. 56, no. 5, pp. 5565-5574, 2020, doi: 10.1109/TIA.2020.3004294.

[46] J. Meng *et al.*, "An Overview and Comparison of Online Implementable SOC Estimation Methods for Lithium-ion Battery," *IEEE Transactions on Industry Applications,* vol. 54, no. 2, pp. 1583-1591, 2018.

[47] B. Arabsalmanabadi, N. Tashakor, S. Goetz, and K. Al-Haddad, "Li-ion Battery Models and A Simplified Online Technique to Identify Parameters of Electric Equivalent Circuit Model for EV Applications," presented at the IECON 2020 The 46th Annual Conference of the IEEE Industrial Electronics Society, 18-21 Oct. 2020, 2020.

[48] F. Rong, X. Gong, X. Li, and S. Huang, "A New Voltage Measure Method for MMC Based on Sample Delay Compensation," *IEEE Transactions on Power Electronics,* vol. 33, no. 7, pp. 5712-5723, 2018, doi: 10.1109/TPEL.2017.2748969.

[49] T. Sarkar and S. K. Mazumder, "Optimum input-filter-capacitor sizing for fuel-cell based single-phase inverter for current-ripple mitigation," presented at the Proceedings of the 2011 14th European Conference on Power Electronics and Applications, 30 Aug.-1 Sept. 2011, 2011.

[50] S. De Breucker, K. Engelen, R. D'hulst, and J. Driesen, "Impact of Current Ripple on Li-ion Battery Ageing," *World Electric Vehicle Journal,* vol. 6, no. 3, 2013, doi: 10.3390/wevj6030532.

[51] F. Chang, F. Roemer, and M. Lienkamp, "Influence of Current Ripples in Cascaded Multilevel Topologies on the Aging of Lithium Batteries," *IEEE Transactions on Power Electronics,* vol. 35, no. 11, pp. 11879-11890, 2020, doi: 10.1109/TPEL.2020.2989145.

[52] T. Kacetl, J. Kacetl, N. Tashakor, M. Jaensch, and S. Goetz, "Degradation-Reducing Control for Dynamically Reconfigurable Batteries," *arXiv preprint arXiv:2202.11757,* 2022.